Available online at www.sciencedirect.com

ScienceDirect

Procedia Structural Integrity 38 (2022) 109–115

Structural Integrity Procedia

www.elsevier.com/locate/procedia

FATIGUE DESIGN 2021, 9th Edition of the International Conference on Fatigue Design

Room Temperature Mechanical Properties of Additively Manufactured Ni-base Superalloys: A Comparative Study

Reza Ghiaasiaan[a,b], Arun Poudel[a,b], Nabeel Ahmad[a,b], Muztahid Muhammad[a,b], Paul R. Gradl[c], Shuai Shao[a,b], Nima Shamsaei [a,b,*]

[a]*Department of Mechanical Engineering, Auburn University, Auburn, AL 36849, USA*
[b]*National Center for Additive Manufacturing Excellence (NCAME), Auburn University, Auburn, AL 36849, USA*
[c]*NASA Marshall Space Flight Center, Propulsion Department, Huntsville, AL 35812, USA*

Abstract

The unique layer-by-layer manufacturing strategy and near-net shaping capability of Additive Manufacturing (AM) make it a promising technology for Ni-superalloys components, where their typical service conditions demand complex shapes and impose significant production costs due to the alloys' poor machinability. In this work, the room temperature mechanical behavior of several Ni-superalloys, including Hastelloy X, Inconel 718, and Inconel 625, were investigated and their properties/performances compared. The test specimens were produced using various AM processes such as laser powder bed fusion (L-PBF) and/or laser powder direct energy deposition (LP-DED). Thorough analyses on microstructures as well as mechanical performance under static/cyclic axial loads have been performed on test specimens. This study aimed to provide a better understanding of process-structure-property relationship for the AM processed Ni-superalloys in two steps. In the process-structure step: the microstructural evolution as the result of thermal cycles has been studied by quantitative metallography based on scanning electron microscopy (SEM). In the structure-property step: both measured fatigue and tensile properties were attempted to be correlated with microstructure.

Keywords: Laser powder bed fusion (L-PBF); Laser powder direct energy deposition (LP-DED) Ni-base superalloys; Fatigue

* Corresponding author. Tel.: +1-334-844-4839; fax: +1-334-844-3307.
E-mail address: shamsaei@auburn.edu

10.1016/j.prostr.2022.03.012

1. Introduction

In recent years, the low cycle fatigue (LCF) behavior of additively manufactured (AM) materials has received a great deal of attention. There is considerable interest in the LCF of AM Ni-base superalloys not only from a fundamental point of view, but also the practical and engineering viewpoint. For instance, it is recognized that the LCF performance of Ni-base alloys can be a limiting factor in alloy selection for many cases of turbine engines (Donachie and Donachie, 2002). A number of works have been written concerning the LCF of Ni-base alloys in both AM and wrought conditions at both ambient and elevated temperatures (Avery *et al.*, 2018; Kim *et al.*, 2020; Lindström *et al.*, 2020; Nezhadfar, Johnson and Shamsaei, 2020).

In this study, the microstructures of AM Ni-base superalloys such as L-PBF/LP-DED IN 718, L-PBF/LP-DED Hastelloy X and L-PBF/LP-DED IN 625 are presented and their fatigue behaviors are compared at two strain amplitudes of 0.005 and 0.01 mm/mm.

2. Experimental Procedure

The LP-DED and L-PBF test specimens were fabricated by the RPM Innovations (Rapid City, SD) and Carpenter Additive (Philadelphia, PA), respectively, using the process parameters listed in Table 1. Further, Table 2 and Fig. 1 presents the chemical compositions of the powders measured by inductively coupled plasma (ICP) spectroscopy methods and reported by the manufacturer. The heat treatment procedures performed in this study are presented in Table 3 as well as Fig. 2. The test specimens were heat treated in a vacuum furnace using an external thermocouple attached to the specimens to maintain the temperature deviation during the heat treatment within ±5 °C from the set temperature of the furnace. The heat treatment procedures was performed according to the ASTM F3055-14a (ASTM International, 2014a) for AM IN 718, the ASTM F3056-14a (ASTM International, 2014b). for AM IN 625 and the ASTM B572-06 (2016) (ASTM International, 2016).

Table 1. AM process parameters used for fabrication of Ni-base superalloy test specimens.

Process	Power (W)	Layer height (μm)	Travel speed (mm/min)
LP-DED	1070	381	1016
L-PBF	180-200	30-40	60,000

Table 2. Chemical composition in wt.% of a few Ni-base superalloy powders used for fabrication of the AM specimens used in this study.

Powder	Ni	Cr	Mo	Co	Fe	Nb+Ta	Ti+Al	Powder Manufacturer
IN 718	52.5	19	3.1	1	16.8	5	1.5	AP&C (a GE additive company)
Hastelloy X	49.1	21.8	9	-	18.5	-	-	Visser Precision
IN 625	63	21.5	9	1	5	3.7	0.8	Visser Precision

Further microstructural analysis was performed on small coupons cut from heat treated test specimens, in the normal direction (ND) plane, i.e., the plane perpendicular to the build direction. The microstructural coupons were later mounted, ground, and polished according to ASTM-E3 (ASTM International, 2012). A Zeiss Crossbeam 550 scanning electron microscope (SEM) equipped with energy dispersive spectroscopy (EDS) and Electron backscatter diffraction (EBSD) detectors was used for further microstructural analysis. Backscattered secondary electron (BSE) micrographs were obtained using the electron channeling contrast imaging (ECCI) technique (Zaefferer and Elhami, 2014).

Table 3. List of heat treatment processes used in this study for the Ni-base superalloys investigated.

Materials	Stress Reliving (SR)	Hot Isostatic Pressing (HIP)	Solutionizing (SOL)	Ageing	
				1-step (A1)	2-step (A2)
	Temperature-°C/Holding Time-hr/(Pressure-MPa)/Quench Medium				
IN 718	1066°C /1.5h/Argon	1165°C /3.5h/100MPa/AC	1165°C /1h/Argon	760°C /10h/Furnace	649°C /10h/Air
IN 625			1177°C /1h/Argon	NA	
Hastelloy X			1177°C /3h/Argon	NA	

Uniaxial, fully-reversed ($R_\varepsilon = \varepsilon_{min}/\varepsilon_{max} = -1$), strain-controlled fatigue tests were performed on the fatigue specimens at room temperature at the strain amplitudes of 0.005 and 0.01 mm/mm according to the ASTM E606 standard (ASTM International, 2019). Tests were considered concluded upon final fracture. If any tests exceeded 10^7 reversals, they were terminated and considered as run outs.

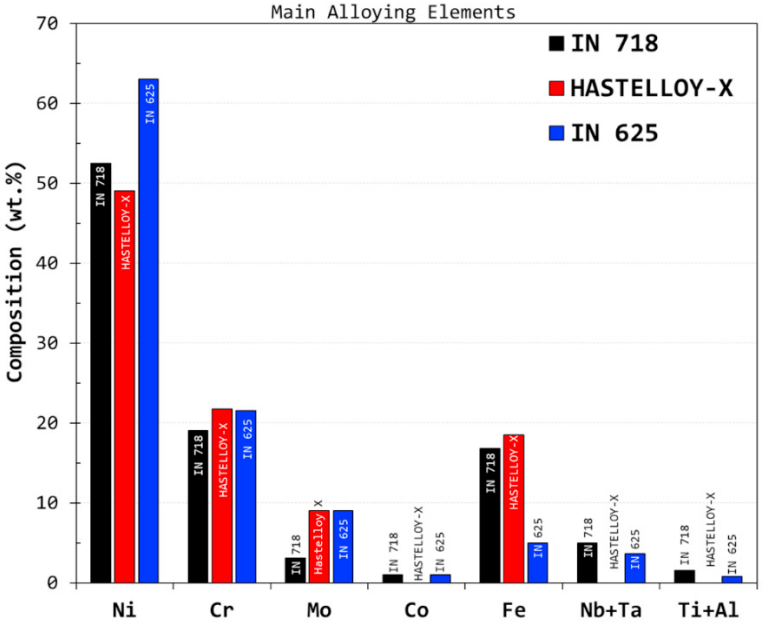

Fig. 1. Comparative bar chart of the main alloying elements for some Ni-base superalloys investigated in this study. Note the chemical compositions were reported by the manufacturers of the powders.

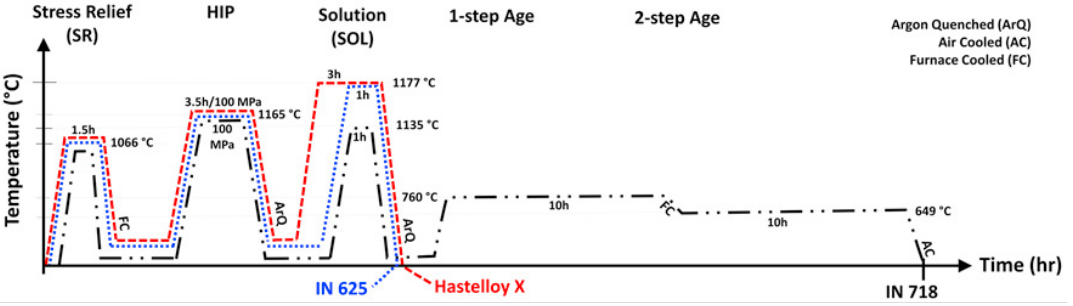

Fig. 2. Schematic diagram for the heat treatment schedules used for the AM Ni-base superalloy specimens investigated in this study.

3. Results and Discussion

Inverse pole figure (IPF) maps obtained in normal direction (ND) plane from EBSD analysis for the non-heat treated (NHT) and fully heat-treated conditions of all the AM Ni-base superalloys investigated in this study are presented in Fig. 3. It should be noted that the average grain size measured as circular equivalent diameter by the EBSD analysis are also reported on the IPF maps shown in Fig. 3. As shown, the grain sizes are slightly increased after heat treatments for all the Ni-base superalloys investigated in this study. Further, it is also notable that the grain size for the Ni-base superalloys fabricated by the LP-DED process are slightly larger that of the L-PBF counterparts, which could be attributed to high cooling rate experienced during the L-PBF process (Liu and Shin, 2019) as well as higher deposition layer height used during the fabrication process of the LP-DED specimens.

The typical BSE SEM micrographs obtained in ND plane from EBSD analysis for the non-heat treated (NHT) and fully heat-treated conditions of all the AM Ni-base superalloys investigated in this study are presented in Fig. 4. As shown, upon heat treatment, the prior inter-dendritic regions observed in NHT condition are significantly removed for most of the AM Ni-base superalloys investigated. However, it seems for some there are some remnants of prior inter dendritic regions discernible in the BSE micrographs such as for LP-DED Hastelloy X, as shown in Fig. 4 (g)-(i). It should also be noted the IN 718 is a precipitation hardening Ni-base superalloy, and the plate-like ɣ”-precipitates in IN 718 were observed in the BSE micrographs, as shown in Fig. 4 (c).

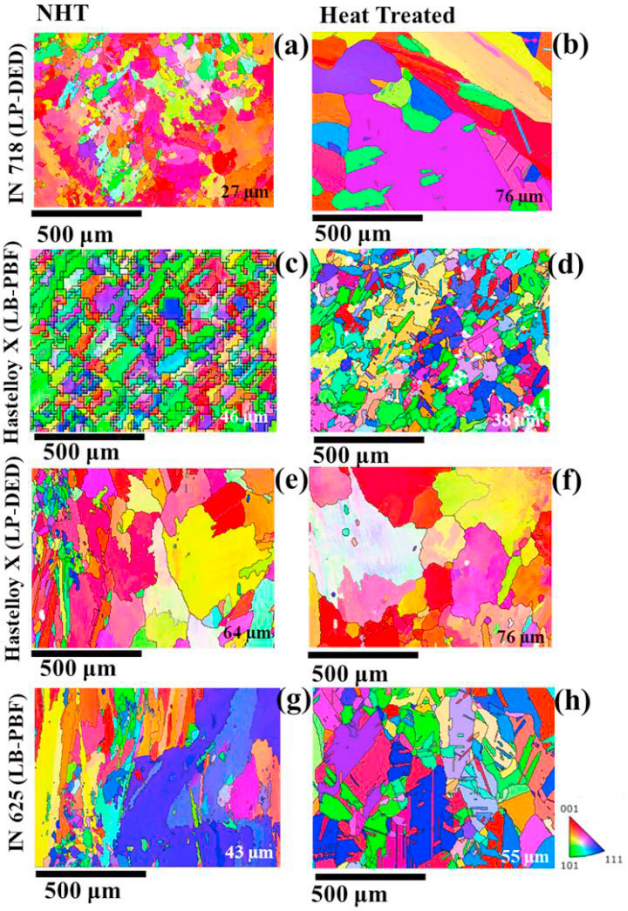

Fig. 3. Inverse pole figure (IPF) maps obtained in the ND plane (perpendicular to building direction) for some Ni-base superalloys investigated in this study in two conditions, i.e., non-heat treated (NHT) and fully heat treated conditions as listed in Table 3: (a)-(b) LP-DED IN 718, (c)-(d) L-PBF Hastelloy X, (e)-(f) LP-DED Hastelloy X, and (g)-(h) LP-DED IN 625.

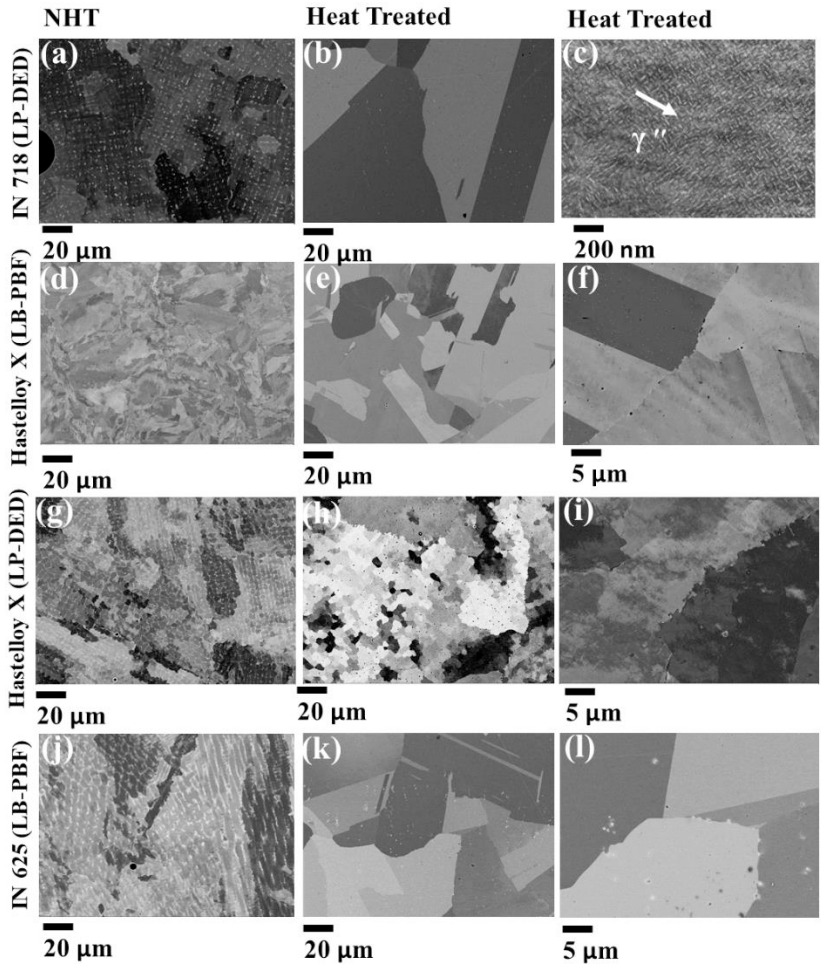

Fig. 4. Typical BSE SEM micrographs obtained in the ND plane (perpendicular to building direction) for some Ni-base superalloys investigated in this study in two conditions, i.e., non-heat treated (NHT) and fully heat treated conditions as listed in Table 2: (a)-(c) LP-DED IN 718, (d)-(f) L-PBF Hastelloy X, (g)-(i) LP-DED Hastelloy X, and (j)-(l) LP-DED IN 625.

The fatigue lives (reversals to failure, $2N_f$) at two different strain amplitudes (i.e., ε_a=0.005 and 0.01 mm/mm) for the Ni-base superalloys investigated in this study in fully heat-treated conditions are presented in Fig. 5 (a). The ranges of fatigue lives ($2N_f$) are presented using bars whose ends indicate the maximum and minimum lives observed for each specimen condition. This figure indicated that, in general, the solid solution strengthened Ni-base superalloys (Hastelloy X and IN 625) have be better fatigue performance as compared to the precipitation hardening counterparts (such as IN 718) in the LCF regime. Specifically, the LP-DED Hastelloy X and LP-DED IN 625 alloys have shown better fatigue performance than the LP-DED/L-PBF IN 718, at both strain amplitudes (i.e., ε_a = 0.01 and 0.005 mm/mm, which could be possibly attributed to the superior ductility of the IN 626 and Hastelloy X compared to IN 718.

This difference in ductility may be related to the presence of ɣ”-strengthening precipitates in LP-DED/L-PBF IN 718, and the absence of any major strengthening phases in Hastelloy X and IN 625 alloys (see Fig. 4). Better ductility can give rise to larger plastic zones at the crack tips and better resistance to fatigue crack propagation which govern the LCF lives. From Fig. 5 (a) that it seems that all the Ni-base alloys investigated have shown slightly better fatigue performance at both strain amplitudes in LP-DED condition as compared with the L-PBF

counterparts. However, at the lower strain amplitude (ε_a = 0.005 mm/mm), IN 625 seems to have a moderately more scattered data points in L-PBF condition, which outperformed the LP-DED counterpart. This could possibly be ascribed to the effect of larger and more uniform grain size in the LP-DED condition, leading to moderately improved and more consistent fatigue performance of the alloy.

Furthermore, the stress response at midlife for all the Ni-base alloys investigated in this study are compared in Fig. 5 (b). As shown, the ɣ”-strengthened IN 718 in both L-PBF and LP-DED conditions have shown significantly higher stress levels at midlife as compared with the solid solution Ni-base alloys investigated in this study, i.e., Hastelloy X and IN 625, which is an indicative of higher load bearing capability of the formers. This could possibly be ascribed to higher strengths in the IN 718 alloys due to the precipitation hardening effect of strengthening ɣ”-phases.

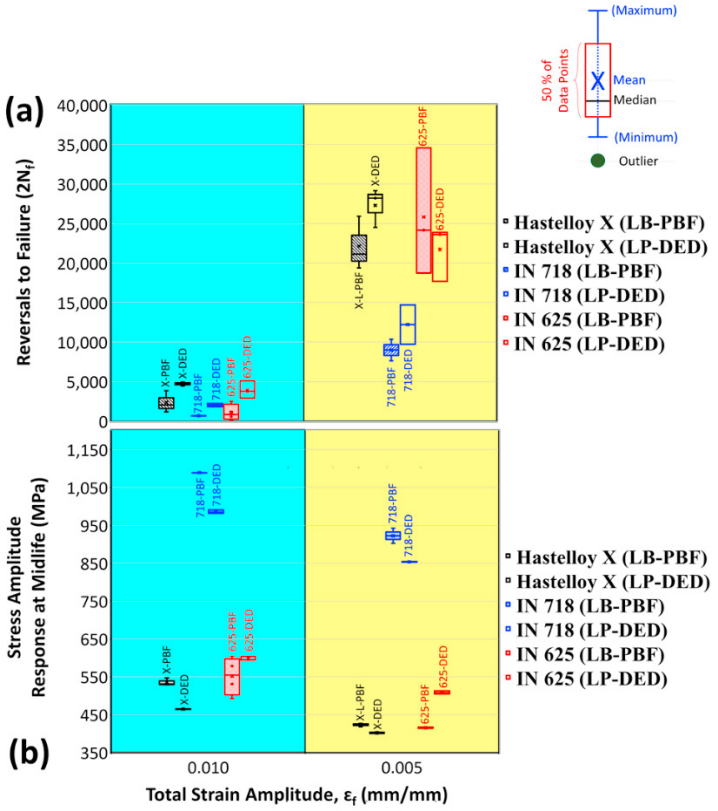

Fig. 5. Room temperature average stress amplitude measured for midlife cycle in (a) and average fatigue lives in (b) at two different strain amplitudes, i.e., ε_a = 0.005 and 0.01 mm/mm, for different additively manufactured Ni-base alloys investigated in this study in fully heat-treated conditions, including L-PBF/LP-DED IN 718, L-PBF/LP-DED Hastelloy X, and L-PBF/LP-DED IN 625.

4. Summary and Conclusions

In this study, the room temperature fatigue behaviors of a few additively manufactured Ni-base superalloys including L-PBF/LP-DED IN 718, L-PBF/LP-DED Hastelloy X and L-PBF/LP-DED IN 625 were investigated and compared at two stain amplitudes of 0.005 and 0.01 mm/mm along with their initial microstructure in non- and fully heat-treated conditions. The test specimens were heat treated using a multiple-step procedure including the stress relieved at 1066 °C for 1.5 hr, followed by HIP at 1065 °C for 3.5 hr under 100 MPa plus solution treatment at 1135 °C (for 3 hr for IN 625) and 1177 °C (for 1 hr for IN 718 and for 3 hr for IN 625) and plus standard 2-step ageing processes (for IN 718). A summary of the experimental observations obtained in this study is listed below:

- The BSE micrographs reveal that the grain structure of the Ni-base superalloys investigated are slightly homogenized and the prior inter dendritic regions are significantly dissolved upon the heat treatments. However, it seems that the microstructure of the alloys manufactured by the LP-DED process possess slightly larger grain sizes than those of the L-PBF counterparts, which could be attributed to the higher cooling rate experienced during the L-PBF process as well as higher layer height used in fabrication process of the LP-DED specimens.
- The comparison of fatigue lives of the Ni-base alloys revealed that at both strain amplitudes (i.e., ε_a=0.01 and 0.005 mm/mm), the L-PBF/LP-DED IN 625 and LP-DED/L-PBF Hastelloy X alloys have shown moderately better fatigue performance than the LP-DED/L-PBF IN 718, which could be possibly attributed to the better ductility of the former two alloys.
- Furthermore, from fatigue lives comparison, it seems that all the Ni-base alloys investigated have shown slightly better fatigue performance at both strain amplitudes in LP-DED condition as compared with the L-PBF counterparts, which could possibly be ascribed to the effect of larger grain size in the LP-DED materials, leading to moderately better improved ductility of the alloy.

Acknowledgements

This material is based upon the work partially supported by the National Aeronautics and Space Administration (NASA) under Cooperative Agreement No. 80MSFC19C0010. This paper describes objective technical results and analysis. Any subjective views or opinions that might be expressed in the paper do not necessarily represent the views of the National Aeronautics and Space Administration (NASA) or the United States Government.

References

ASTM International (2012) ‘ASTM E3-11: Standard Guide for Preparation of Metallographic Specimens’. doi: 10.1520/E0003-11R17.1.

ASTM International (2014a) ‘ASTM F3055-14a Standard Specification for Additive Manufacturing Nickel Alloy (UNS N07718) with Powder Bed Fusion’. doi: 10.1520/F3055-14A.

ASTM International (2014b) ‘ASTM F3056-14a: Standard Specification for Additive Manufacturing Nickel Alloy (UNS N06625) with Powder Bed Fusion’. doi: 10.1520/F3056-14E01.

ASTM International (2016) ‘ASTM B572-06(2016): Standard Specification for UNS N06002, UNS N06230, UNS N12160, and UNS R30556 Rod’. doi: 10.1520/B0572-06R16.

ASTM International (2019) ‘E606/E606M - 19e1: Standard Test Method for Strain-Controlled Fatigue Testing’. doi: 10.1520/E0606_E0606M-19E01.

Avery, D. Z. *et al.* (2018) ‘Fatigue Behavior of Solid-State Additive Manufactured Inconel 625’, *JOM*, 70(11), pp. 2475–2484. doi: 10.1007/s11837-018-3114-7.

Donachie, M. J. and Donachie, S. J. (2002) *Superalloys: A Technical Guide*. 2nd edn, *America*. 2nd edn. Materials Park, OH: ASM International. doi: 10.1361.

Kim, K.-S. *et al.* (2020) ‘High-temperature tensile and high cycle fatigue properties of inconel 625 alloy manufactured by laser powder bed fusion’, *Additive Manufacturing*, 35, p. 101377. doi: 10.1016/j.addma.2020.101377.

Lindström, T. *et al.* (2020) ‘Fatigue behaviour of an additively manufactured ductile gas turbine superalloy’, *Theoretical and Applied Fracture Mechanics*, 108, p. 102604. doi: 10.1016/j.tafmec.2020.102604.

Liu, S. and Shin, Y. C. (2019) ‘Additive manufacturing of Ti6Al4V alloy: A review’, *Materials and Design*. The Authors, 164, p. 107552. doi: 10.1016/j.matdes.2018.107552.

Nezhadfar, P. D., Johnson, A. S. and Shamsaei, N. (2020) ‘Fatigue behavior and microstructural evolution of additively manufactured Inconel 718 under cyclic loading at elevated temperature’, *International Journal of Fatigue*, 136, p. 105598. doi: 10.1016/j.ijfatigue.2020.105598.

Zaefferer, S. and Elhami, N.-N. (2014) ‘Theory and application of electron channelling contrast imaging under controlled diffraction conditions’, *Acta Materialia*, 75, pp. 20–50. doi: 10.1016/j.actamat.2014.04.018.